JOURNAL OF AIRCRAFT
Vol. 48, No. 4, July–August 2011

Research on a New Aircraft Point-Mass Model

Fumiaki Imado*
Shinshu University, Nagano 380-8553, Japan
Yuki Heike†
All Nippon Airways Company, Ltd., Tokyo 144-0041, Japan
and
Takuya Kinoshita‡
Ministry of Defense, Tokyo 162-8804, Japan

DOI: 10.2514/1.C000200

Up to now in the field of aeronautics, point-mass models have been widely employed for missiles and aircraft. In the case of missiles, there have been no problems; however, in solving aircraft optimal control problems (in particular, under windy conditions), the authors could not find a reliable model in the existing point-mass models. Therefore, a new aircraft point-mass model has been developed in the authors' laboratory. This model employs angle of attack, sideslip angle, bank angle, and thrust as four control variables. The existing models cannot precisely introduce the effect of natural winds or active sideslip-angle control, while this new model can introduce them with precision. This model was applied to a YF-16 aircraft, and the precision was investigated by comparing the results with that of the rigid-body model. The comparisons of step responses and simulations for typical maneuvers showed the precision and the reliability of this model.

Nomenclature

b	=	wing span, m
C	=	side force, N
C_C	=	side force coefficient
C_D	=	drag force coefficient
C_L	=	lift force coefficient
C_l	=	rolling moment coefficient
C_m	=	pitching moment coefficient
C_n	=	yawing moment coefficient
C_X	=	X force coefficient
C_Y	=	Y force coefficient
C_Z	=	Z force coefficient
C'	=	side force in wind axes
$\bar{c}$	=	wing mean aerodynamic chord, m
D	=	drag force, N
D'	=	drag force in wind axes, N
E, E_1, E_2	=	transformation matrices
g	=	gravitational constant, 9.8 m/s^2
h	=	altitude, m
I_X, I_Y, I_Z, I_{XZ}	=	aircraft inertial matrix components, kg m^2
k_{p1}, k_{p2}, k_{r1}, k_{r2}, k_{r3}, T_0, T_1, T_2	=	parameters of lateral-directional autopilot
k_T	=	parameter of velocity-control autopilot
k_1, k_2, k_3, k_4, k_5	=	parameters of longitudinal autopilot
L	=	lift force, N
L'	=	lift force in wind axes, N
m	=	aircraft mass, kg
P_1, P_3	=	engine input and its output, %
p, q, r	=	angular velocity components in body coordinates, /s
Q	=	dynamic pressure, kg/m/s^2
S	=	reference area, m^2
u, v, w	=	velocity components in body coordinates, m/s
T, T_c	=	thrust and its command, N
T_{bias}, T_{st}	=	gravitational and aerodynamic compensation terms of thrust command, N
V, V_c	=	aircraft inertial velocity and its command, m/s
V_a	=	relative air velocity, m/s
V_{ax}, V_{ay}, V_{az}	=	components of relative air velocity, m/s
V'_w	=	wind velocity, m/s
V'_{wx}, V'_{wy}, V'_{wz}	=	components of wind velocity, m/s
x, y, z	=	inertial coordinates, m
x_b, y_b, z_b	=	body coordinates, m
α, α_c	=	angle of attack and its command
α_{eff}	=	effective angle of attack
β, β_c	=	sideslip angle and its command
β_{eff}	=	effective sideslip angle
γ	=	inertial flight-path angle
δ_a	=	aileron angle
δ_h, δ_{hc}	=	elevator angle and its command
δ_r	=	rudder angle
θ	=	pitch angle
ρ	=	air density, kg/m^3
τ_α, τ_β, τ_ϕ	=	time constants for α, β, and ϕ, s
Φ_b	=	body coordinate frame
Φ_I	=	inertial coordinate frame
Φ_w	=	wind-axes coordinate frame
ϕ, ϕ_c	=	bank angle and its command
φ	=	roll angle
ψ	=	yaw angle

Subscripts

b	=	body coordinate frame
c	=	command signal
w	=	wind-axes coordinate frame

Received 30 November 2009; revision received 21 March 2011; accepted for publication 22 March 2011.

*Professor, Department of Mechanical Systems Engineering; imadofu@shinshu-u.ac.jp. Senior Member AIAA.
†Engineer, Engineering and Maintenance; y.heike@ana.co.jp.
‡Major, Air Staff Office, Air Self Defense Force; asdd2103@aso.mod.go.jp.

I. Introduction

UNTIL now, in studies of the guidance control systems of aircraft and missiles, point-mass models with three control variables

[1–13] have usually been employed. In these models, attitude control systems called "autopilots" are incorporated, and through these autopilots, it is assumed that the attitude is quickly controlled. Therefore, in many cases, the vehicle is approximated by a point mass, and only its translational motion is considered in designing flight control systems. An aircraft point-mass model often employs angle of attack α, bank angle ϕ, and thrust T as three control variables, and sideslip angle β is controlled to 0, which is the assumption of a coordinated turn [14]. This point-mass model is mathematically accurate so far as β is 0. Other existing point-mass models that employ three control variables α, β, and T are not accurate because they usually employ the assumption of a small β. The authors have been studying aircraft optimal guidance and trajectory control systems in the presence of wind. In the prestudy investigation, when the effect of a natural wind is to be considered, usually a rigid-body model has been employed, and studies using a precise point-mass model employing α, β, ϕ, and T were not found. When using a point-mass model, a larger time interval for the numerical integration can be selected than with a rigid-body model. The number of states to be integrated is also smaller than with the rigid-body model; therefore, the integration is implemented in a shorter time by the point-mass model. However, modern PCs can conduct integration very rapidly; therefore, it is not an important point. The time interval employed in this paper is 1 ms, which is far smaller than the required interval (10 ms will be enough to maintain the precision of the numerical integration). On the other hand, existent solvers for nonlinear optimal control problems limit the number of time steps to at most 200. With so few small time steps, the short period mode included in a rigid-body model makes it impossible to calculate the optimal flight trajectory for a long period (e.g., 100 s), while by employing the point-mass model, it is possible. This is one of the great advantages of the point-mass model. A preliminary design of the aircraft trajectory control system is easier when employing the point-mass model than with the rigid-body model. This is another advantage of the point-mass model. Throughout investigations, the authors could not find any precise point-mass models that employ four control variables α, β, ϕ, and T, so the authors derived an accurate new point-mass model in the laboratory. As point-mass models are approximations of a rigid-body model, the accuracy should be examined. This point has often been neglected in preceding studies. In this paper, the accuracy of the derived model is thoroughly examined by comparing it with the rigid-body model, and the reliability of employing this model is verified. That is, the control-signal commands are first obtained by this point-mass model. Then they are applied to the rigid-body aircraft model, and the obtained aircraft motions are examined. In Sec. II, the derived point-mass model with four control variables is explained. To examine the applicability of this model, the same commands have to be applied to this point-mass model and to the rigid-body model, and the results have to be compared. For this purpose some control systems of the rigid-body aircraft have to be designed so that it follows the above signals. In Sec. III, these control systems are explained. Three typical aircraft maneuvers are selected, and a comparison study is conducted in Sec. IV. The results are briefly summarized as conclusions in Sec. V.

II. Derivation of the New Point-Mass Model

The equations of motion for the rigid-body model [14–19] have appeared in many texts and papers (e.g., in [15]); therefore, these equations are only presented here for the readers' convenience.

Translational motions:

$$\dot{u} = rv - qw - g\sin\theta + \frac{QS}{m}C_X + \frac{T}{m} \tag{1}$$

$$\dot{v} = pw - ru + g\cos\theta\sin\phi + \frac{QS}{m}C_Y \tag{2}$$

$$\dot{w} = qu - pv + g\cos\theta\cos\phi + \frac{QS}{m}C_Z \tag{3}$$

$$\dot{x} = u\cos\theta\cos\psi + v(-\cos\phi\sin\psi + \sin\phi\sin\theta\cos\psi) + w(\sin\phi\sin\psi + \cos\phi\sin\theta\cos\psi) \tag{4}$$

$$\dot{y} = u\cos\theta\sin\psi + v(\cos\phi\cos\psi + \sin\phi\sin\theta\sin\psi) + w(-\sin\phi\cos\psi + \cos\phi\sin\theta\sin\psi) \tag{5}$$

$$\dot{z} = -u\sin\theta + v\sin\phi\cos\theta + w\cos\phi\cos\theta \tag{6}$$

where $\dot{u}$, $\dot{v}$, and $\dot{w}$ are the three aircraft velocity components; C_X, C_Y, and C_Z are the aerodynamic force coefficients in the aircraft body axes x_b-y_b-z_b, respectively; S is the wing area; and Q is the dynamic pressure, the exact definition of which will be given in a later part of this section [Eq. (32)].

Rotational motions:

$$\dot{p} = \frac{I_Y - I_Z}{I_X}qr + \frac{I_{XZ}}{I_X}(\dot{r} + pq) + \frac{QSb}{I_X}C_l \tag{7}$$

$$\dot{q} = \frac{I_Z - I_X}{I_Y}pr + \frac{I_{XZ}}{I_Y}(r^2 - p^2) + \frac{QS\bar{c}}{I_Y}C_m \tag{8}$$

$$\dot{r} = \frac{I_X - I_Y}{I_Z}pq + \frac{I_{XZ}}{I_Z}(\dot{p} - qr) + \frac{QSb}{I_Z}C_n \tag{9}$$

$$\dot{\phi} = p + (q\sin\phi + r\cos\phi)\tan\theta \tag{10}$$

$$\dot{\theta} = q\cos\phi - r\sin\phi \tag{11}$$

$$\dot{\psi} = (q\sin\phi + r\cos\phi)\sec\theta \tag{12}$$

where I_X, I_Y, I_Z, and, I_{XZ} are the components of the aircraft inertial matrix; b is the wing span; $\bar{c}$ is the wing mean aerodynamic chord; and C_l, C_m, and C_n are rolling, pitching, and yawing aerodynamic moment coefficients, respectively.

On the other hand, in the new point-mass model, by using the symbols defined in Fig. 1, the equations of motion of the aircraft are given as follows:

$$\dot{V} = \frac{T\cos\phi\cos\beta - D'}{m} - g\sin\gamma \tag{13}$$

$$\dot{\gamma} = \frac{T(\cos\phi\sin\alpha + \sin\alpha\cos\alpha\sin\beta) + L'\cos\phi + C'\sin\phi}{mV} - g\cos\gamma/V \tag{14}$$

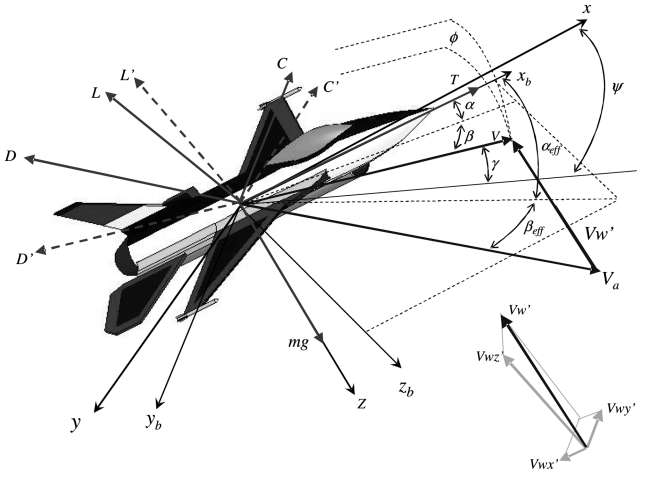

Fig. 1 Some symbols of a new aircraft point-mass model with four control variables.

$$\dot{\psi} = \frac{T(\sin\phi\sin\alpha - \cos\phi\cos\alpha\sin\beta) + L'\sin\phi - C'\cos\phi}{mV\cos\gamma} \quad (15)$$

$$\dot{x} = V\cos\gamma\cos\psi \quad (16)$$

$$\dot{y} = V\cos\gamma\sin\psi \quad (17)$$

$$\dot{h} = V\sin\gamma \qquad (h = -z) \quad (18)$$

The origins of all of the following coordinates are taken at the aircraft center of mass: x, y, z are the inertial coordinate (Φ_I) axes; x_b, y_b, z_b are the aircraft fixed-body coordinate (Φ_b) axes; Φ_I is translated into Φ_b through the successive rotation of the Euler angles ψ (yaw angle), θ (pitch angle); and φ (roll angle) around the z, y, and x axes.

In Fig. 1, V shows the inertial velocity vector of the aircraft. The coordinate system Φ_w is obtained from Φ_I through the successive rotation of ψ (inertial azimuth angle: same as yaw angle), γ (inertial flight-path angle) and ϕ (bank angle) around the z, y, and x axes. The authors called Φ_w the wind axes here. (Note that the roll angle φ is almost the same as the bank angle ϕ, but they are slightly different.) In Φ_w, V is in the direction of the x axis, and the aerodynamic force components in Φ_w are L', C', and D', where L' is in the direction of the negative z axis, C' is in the direction of the negative y axis, and D' is in the direction of the negative x axis. Equations (13–15) are obtained through the force balance along the three axes of Φ_w. The definition of α and β here is as follows. The body coordinate system Φ_b, through the successive rotation of $-\alpha$ and β around the y and z axes, coincides with Φ_w. As there is no general definition of these symbols in the point-mass model with four control variables developed by the authors, these are the definitions employed only in this paper.

The existence of a constant-velocity wind is assumed here. In Fig. 1, V'_w is the velocity vector of the wind, V'_{wx}, V'_{wy}, and V'_{wz} are the three axes components of it. [Note that if the wind is not constant, the derivatives of the wind components appear in the right sides of Eqs. (13–15).] The effective angle of attack and sideslip angles for the aircraft include the components of natural wind and are expressed here as α_{eff}, and β_{eff}, respectively. The mathematical definition of these angles is shown later. The aircraft lift force L, drag force D, and side force C are defined as functions of these angles as follows:

$$L = QSC_L(\alpha_{\text{eff}}, \beta_{\text{eff}}) \quad (19)$$

$$D = QSC_D(\alpha_{\text{eff}}, \beta_{\text{eff}}) \quad (20)$$

$$C = QSC_C(\alpha_{\text{eff}}, \beta_{\text{eff}}) \quad (21)$$

where the aerodynamic force coefficients C_L, C_D, and C_C are determined by simulations so that they can appropriately give forces for both the rigid-body model and the point-mass model. This algorithm is explained in more detail later. The transformations of the aerodynamic force components between the wind axes and the aircraft body axes are given by the following equations:

$$(D', C', L')^T = E(D, C, L)^T \quad (22)$$

$$E = E_1 E_2 \quad (23)$$

$$E_1 = \begin{bmatrix} \cos\alpha\cos\beta & \sin\beta & \sin\alpha\cos\beta \\ -\cos\alpha\sin\beta & \cos\beta & -\sin\alpha\sin\beta \\ -\sin\alpha & 0 & \cos\alpha \end{bmatrix} \quad (24)$$

$$E_2 = \begin{bmatrix} \cos\alpha_{\text{eff}}\cos\beta_{\text{eff}} & -\cos\alpha_{\text{eff}}\sin\beta_{\text{eff}} & -\sin\alpha_{\text{eff}} \\ \sin\beta_{\text{eff}} & \cos\beta_{\text{eff}} & 0 \\ \sin\alpha_{\text{eff}}\cos\beta_{\text{eff}} & \sin\alpha_{\text{eff}}\sin\beta_{\text{eff}} & \cos\alpha_{\text{eff}} \end{bmatrix} \quad (25)$$

The effective angle of attack, the effective sideslip angle, the aircraft relative velocity to air and its three components, and the dynamic pressure are given as follows:

$$\alpha_{\text{eff}} = \tan^{-1}\left(\frac{V\sin\alpha\cos\beta - V'_{wz}}{V\cos\alpha\cos\beta - V'_{wx}}\right) \quad (26)$$

$$\beta_{\text{eff}} = \sin^{-1}\left(\frac{V\sin\beta - V'_{wy}}{V_a}\right) \quad (27)$$

$$V_a = \sqrt{V_{ax}^2 + V_{ay}^2 + V_{az}^2} \quad (28)$$

$$V_{ax} = V\cos\alpha\cos\beta - V'_{wx} \quad (29)$$

$$V_{ay} = V\sin\beta - V'_{wy} \quad (30)$$

$$V_{az} = V\sin\alpha\cos\beta - V'_{wz} \quad (31)$$

$$Q = \tfrac{1}{2}\rho V^2 \quad (32)$$

As stated above, in the point-mass model, the rotational dynamics are assumed to be controlled and stabilized in a short time. Therefore, in this model, the dynamics of rotations with autopilots are approximated as first-order time lags as follows:

$$\dot{\alpha} = (\alpha_c - \alpha)/\tau_\alpha \quad (33)$$

$$\dot{\beta} = (\beta_c - \beta)/\tau_\beta \quad (34)$$

$$\dot{\phi} = (\phi_c - \phi)/\tau_\phi \quad (35)$$

where α_c, β_c, and ϕ_c are control commands of their angles, and τ_α, τ_β, and τ_ϕ are equivalent time lags of their control channels.

In this paper, all of the rigid-body model data and the point-mass-model data of the aircraft employed the data of the YF-16 fighter of [15]. The reason for this is that all of the data of this aircraft have been published and any researchers can avail themselves of the same data. In fact, the aerodynamic data of many aircraft are kept in secret and have not been published yet. The characteristics of the thrust command to its output are explained in detail in [15], but in this paper only the step response is shown in Fig. 2, where P1 is the input command, and P3 is the output thrust. In the rigid-body model, all of the aerodynamic coefficients are shown as the table functions of α and β in [15]. On the other hand, in the new point-mass model, the aerodynamic coefficients $C_L(\alpha_{\text{eff}}, \beta_{\text{eff}})$, $C_D(\alpha_{\text{eff}}, \beta_{\text{eff}})$, and $C_C(\alpha_{\text{eff}}, \beta_{\text{eff}})$ and time lags τ_α, τ_β, and τ_ϕ have to be determined so

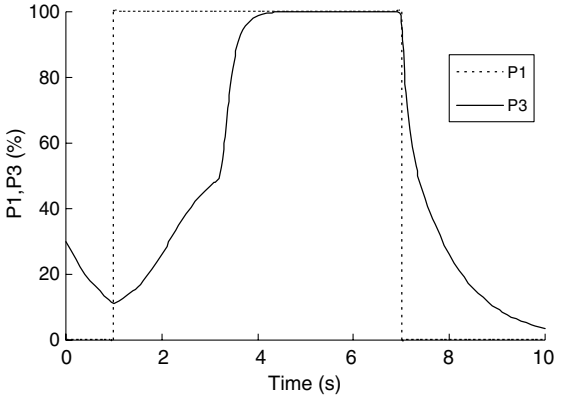

Fig. 2 Step response of the PWF-100 engine.

that the output of the point-mass model coincides with that of the rigid-body model as far as possible. The process is shown in the following.

1) By employing the wind-tunnel test data of [15], estimate the aerodynamic coefficients at coordinate turns $C_L(\alpha_{\text{eff}}, 0)$, $C_D(\alpha_{\text{eff}}, 0)$, and $C_C(\alpha_{\text{eff}}, 0)$. The values of τ_α, τ_β, and τ_ϕ also have to be estimated from the same wind-tunnel test data of [15].

2) By employing the above data, conduct simulations of coordinate turns using the point-mass model. Under the same conditions, conduct simulations of coordinate turns using the rigid-body model.

3) Comparing the time histories of the variables V, γ, ψ, x, y, and h resulting from the two models, revise the parameter values obtained in step 1.

4) By a few iterative corrections of steps 2 and 3, a good estimation of parameters of the point-mass model is obtained in step 1.

5) Next, by employing the obtained data in step 4 and the wind-tunnel test data of [15], estimate the values of $C_L(\alpha_{\text{eff}}, \beta_{\text{eff}})$, $C_D(\alpha_{\text{eff}}, \beta_{\text{eff}})$, and $C_C(\alpha_{\text{eff}}, \beta_{\text{eff}})$.

6) By employing the above parameters, conduct flight simulations using the point-mass model, with several sideslip angles. Conduct flight simulations using the rigid-body model in the same conditions.

7) Comparing the time histories of the variables V, γ, ψ, x, y, and h resulting from the two models, revise the parameter values obtained in step 5.

8) By a few iterative corrections of steps 6 and 7, a good estimation of parameters of the point-mass model is obtained in step 5.

This sequence of processes should be conducted for several flight conditions of aircraft altitude and velocity. An example of the aerodynamic data (at the altitude of 3000 m and the velocity of 200 m/s) that are also employed in the following sections are shown in Table 1, where time lags τ_α, τ_β, and τ_ϕ are assumed to be constant, and the values of 0.4, 0.4, and 0.45 s are employed, respectively.

III. Autopilots of the Rigid-Body Model

In [15], all aerodynamic coefficients are expressed by C_X, C_Y, and C_Z instead of C_L, C_D, and C_C; therefore, for convenience, in the point-mass model, C_X, C_Y, and C_Z values are employed. The transformation between these values is given by the following equations:

$$C_L = C_X \sin\alpha - C_Z \cos\alpha \tag{36}$$

$$C_D = -C_X \cos\alpha \cos\beta - C_Y \sin\beta - C_Z \sin\alpha \cos\beta \tag{37}$$

$$C_C = C_X \cos\alpha \sin\beta - C_Y \cos\beta + C_Z \sin\alpha \sin\beta \tag{38}$$

To compare the point-mass model and the rigid-body model, some autopilots have to be designed and incorporated into the rigid-body model so that the same control command signals can be applied to both models. As the point-mass model in this paper employs α, β, ϕ, and T as control variables, autopilots of the rigid-body model for these commands are designed and incorporated. As it is difficult to control the aircraft velocity directly by the thrust command, the same velocity-control autopilot is incorporated into both the point-mass model and the rigid-body model.

Figure 3 shows the angle-of-attack control autopilot, where δ_h and δ_{hc} are the elevator angle and its command, respectively. This autopilot is designed to use the feedback of α and the pitch rate q in addition to the integral of the error $\alpha - \alpha_c$ in order to eliminate the stationary error. The gain coefficients of the system k_1, k_2, and k_3 are determined by the simulation study. As the coupling effect between β and ϕ is very large, the lateral-directional autopilot shown in Fig. 4 is designed so that they cancel out the coupling effect. In Fig. 4, δ_r and δ_a are the rudder angle and the aileron angle, respectively. The bank-angle control system is designed to use the feedback of ϕ and the roll rate p, and the sideslip-angle control system is designed to use the feedback of β and the yaw rate r with a canceling term for the coupling effect of ϕ. In a horizontal turn, a stationary value of r is required. The direct feedback of r to the rudder causes an extra β and causes the aircraft an undesired motion. To solve this problem, the feedback signal of r is applied through a washout filter. Through this circuit, the rudder responds to only the transient motion of r and does not respond to its stationary value. Figure 2 shows the existence of a large time lag for a thrust input command, which makes it difficult for a pilot to control the aircraft velocity using direct thrust control. Therefore, the velocity-control autopilot shown in Fig. 5 was designed. In this figure, T_{st} and T_{bias} are the terms used to compensate for the aerodynamic drag and the gravity component along the V axis, respectively. The conceptual idea of this system is that by always giving the compensation thrust command for the drag in

Table 1 Aerodynamic coefficients for the point-mass model ($h = 3000$ m, $V = 200$ m/s)

	β						
α	−7.5	−5	−2.5	0	2.5	5	7.5
				C_X			
−10	−0.02394	−0.02638	−0.02502	−0.02413	−0.02395	−0.02403	−0.02148
−5	−0.02364	−0.02437	−0.02514	−0.02607	−0.02472	−0.02341	−0.02196
0	−0.02137	−0.02231	−0.02296	−0.02364	−0.02213	−0.02071	−0.02014
5	−0.00785	−0.00876	−0.00753	−0.00162	−0.00584	−0.00562	−0.00431
10	0.00592	0.00571	0.00711	0.00837	0.00807	0.00787	0.00843
15	0.01093	0.00807	0.00503	0.00225	0.00632	0.00916	0.01003
20	0.01256	0.0112	0.01037	0.00481	0.01055	0.00866	0.00694
				C_Y			
−10	0.05661	0.02428	0.01301	0.00037	−0.01103	−0.01915	−0.04921
−5	0.00832	0.05934	0.03006	−0.00311	−0.02592	−0.04771	−0.07772
0	0.14085	0.16021	0.07885	−0.00374	−0.03074	−0.05807	−0.09157
5	0.09816	0.06522	0.03177	−0.00132	−0.03025	−0.06163	−0.00934
10	0.10169	0.06355	0.03506	0.00555	−0.02124	−0.04693	−0.0884
15	0.09419	0.05773	0.02499	−0.00575	−0.02838	−0.05022	−0.08531
20	0.09038	0.06106	0.02546	−0.00401	−0.03366	−0.05952	−0.09963
				C_Z			
−10	0.81829	0.81859	0.78621	0.7616	0.74738	0.73315	0.71751
−5	0.39639	0.40661	0.3696	0.34916	0.33172	0.30814	0.32795
0	−0.01792	−0.01129	−0.03003	−0.04671	−0.06962	−0.088	−0.07685
5	−0.41566	−0.42431	−0.45424	−0.48248	−0.46921	−0.4516	−0.45508
10	−0.84608	−0.85081	−0.88229	−0.91118	−0.92172	−0.9341	−0.87308
15	−1.30432	−1.28742	−1.28652	−1.27651	−1.35113	−1.35	−1.36811
20	−1.60164	−1.63972	−1.63583	−1.62882	−1.67816	−1.6913	−1.75521

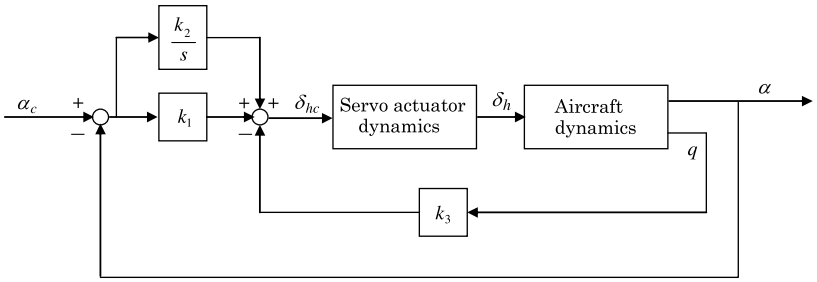

Fig. 3 Block diagram of the longitudinal autopilot.

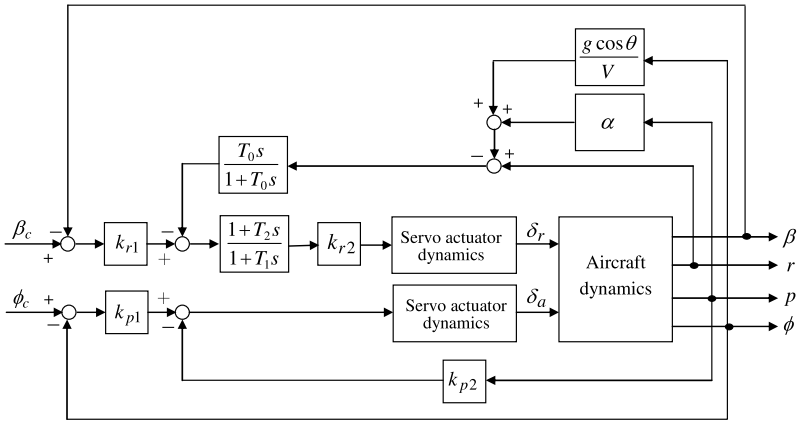

Fig. 4 Block diagram of the lateral-directional autopilot.

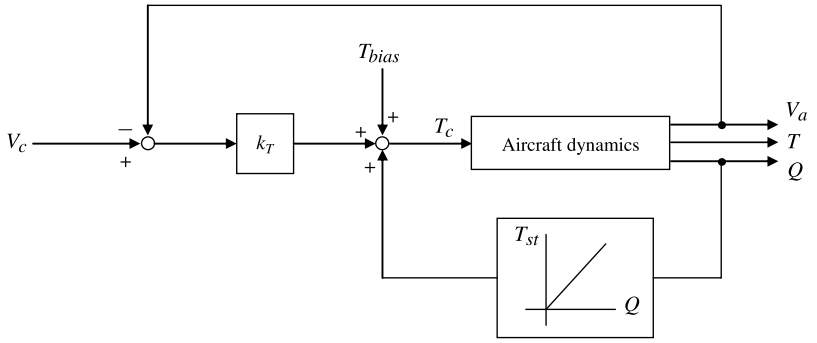

Fig. 5 Block diagram of the velocity-control autopilot.

advance, the system can respond quickly to a request to increase or decrease the aircraft velocity. Figures 6–10 show step responses to the input commands α_c, ϕ_c, β_c, V_c, and T_c, respectively.

IV. Comparative Study Between the Point-Mass Model and the Rigid-Body Model

As the point-mass model obtained above is an approximation of the rigid-body model, the accuracy and the applicability of this model should be examined. For this purpose, the same control-signal commands were applied to both the point-mass and the rigid-body aircraft models, and the resulting aircraft motions were compared. Three typical aircraft maneuvers were selected and a comparative study was conducted in this section.

A. Maneuver 1

With the aircraft maintaining a velocity of 200 m/s, with an angle of attack of 2.5 deg and a sideslip angle of 0 deg, conduct successive left and right horizontal turns using the bank-angle control signal.

Figures 11 and 12 show the flight trajectories in the *x*-*y* plane and the altitude histories. In Fig. 11, the maximum difference between the two models is about 100 m. Considering the flight time and flight distances, this value may be said to be small. In Fig. 12, the altitude histories of both models coincide with each other well. Figures 13–16 show the histories of control variables of both models. These figures show that in the rigid-body model, small overshoots appeared when high-frequency inputs were applied. However, generally speaking, the differences between the two models are small.

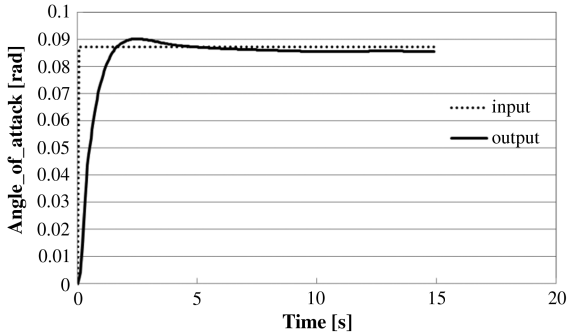

Fig. 6 Step response to the angle-of-attack command (α_c = 0.0873 rad).

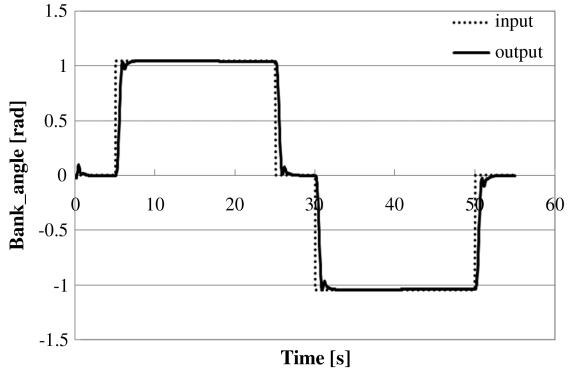

Fig. 7 Step response to the bank-angle command ($\phi_c = 1.0472$ rad).

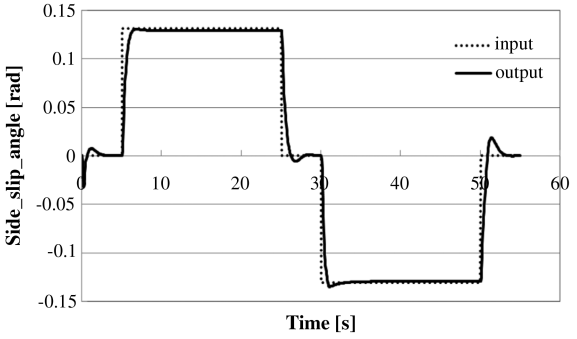

Fig. 8 Step response to the sideslip-angle command ($\beta_c = 0.1309$ rad).

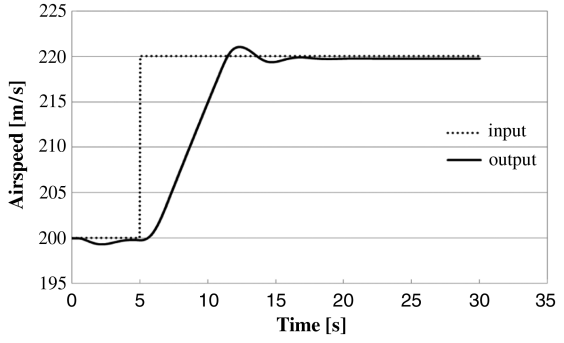

Fig. 9 Step response to the velocity command ($V_c = 220$ m/s).

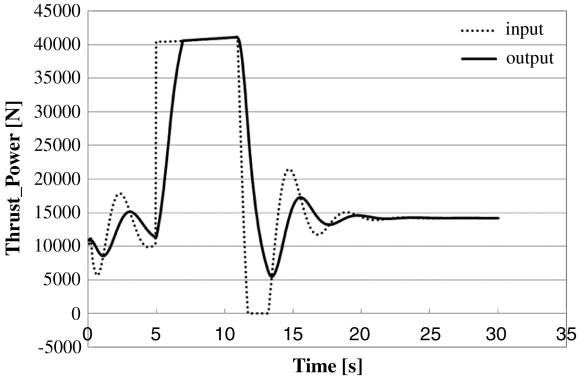

Fig. 10 Step response to the thrust command ($T_c = 40000$ N).

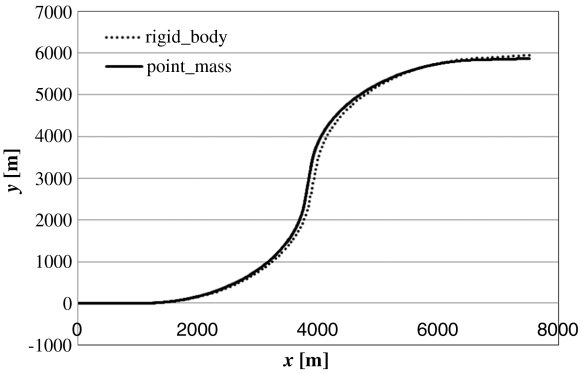

Fig. 11 Trajectories in the x-y plane (maneuver 1).

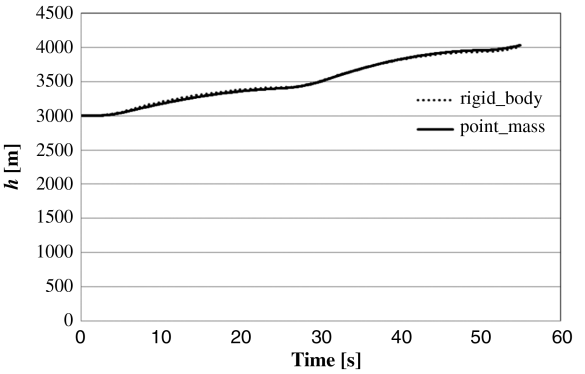

Fig. 12 Altitude histories (maneuver 1).

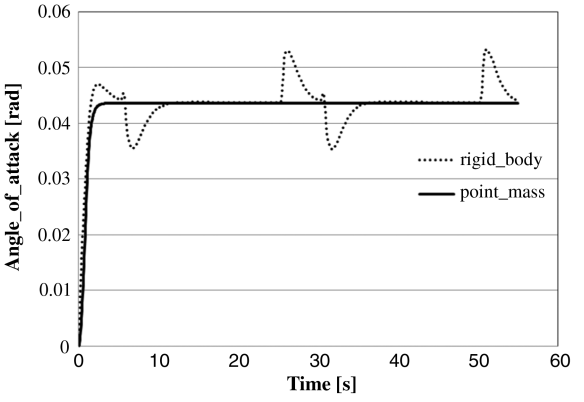

Fig. 13 Angle-of-attack histories (maneuver 1).

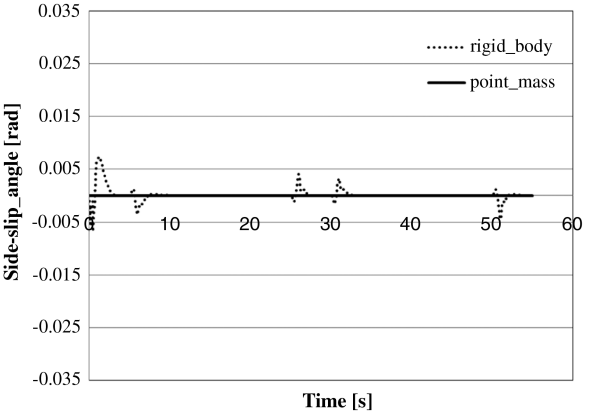

Fig. 14 Sideslip-angle histories (maneuver 1).

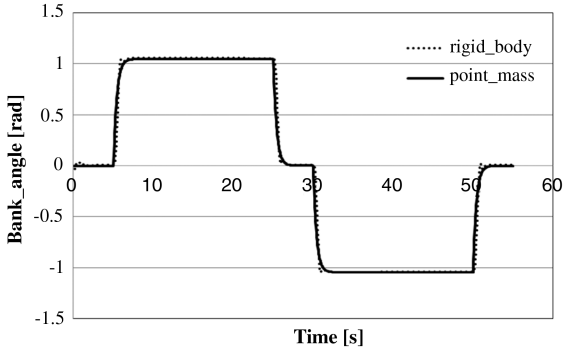

Fig. 15 Bank-angle histories (maneuver 1).

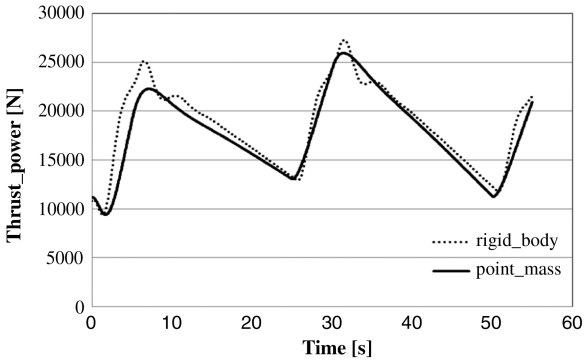

Fig. 16 Thrust histories (maneuver 1).

B. Maneuver 2

With the aircraft maintaining a velocity of 200 m/s, with an angle of attack of 1.25 deg and a bank angle of 0 deg, conduct successive right and left horizontal turns using the sideslip-angle control signal.

Figures 17 and 18 show the flight trajectories in the x-y plane and the altitude histories. In Fig. 17, the maximum difference between the two models is about 120 m. Considering the flight time and flight distances, this value may be said to be small. In Fig. 18, the altitude histories of both models coincide with each other well. Figures 19–22 show the histories of control variables of both models. In the same manner as maneuver 1, these figures show that in the rigid-body model, small overshoots appeared when high-frequency inputs were applied. However, generally speaking, the differences between the two models are small.

The two above maneuvers are selected to show that despite the existence of a strong coupling between β and ϕ, they can control the aircraft independently. Although all of the results are not shown here, other maneuvers studied have shown good coincidence of the results of the two models and, in particular, when a high-frequency input is not included, the coincidence is very good. If required, a position control system can be incorporated into both models; therefore, the deviation of the position will not present any problems. One of these cases is shown in the following maneuver 3.

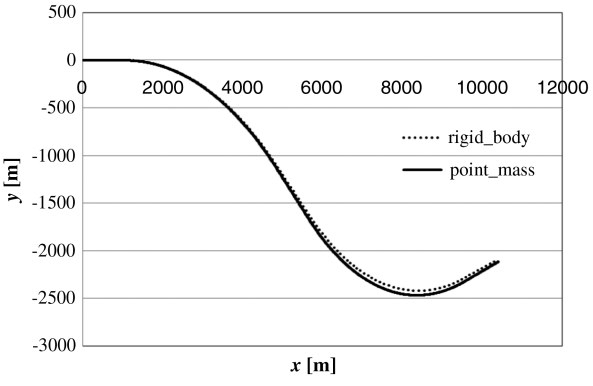

Fig. 17 Trajectories in the x-y plane (maneuver 2).

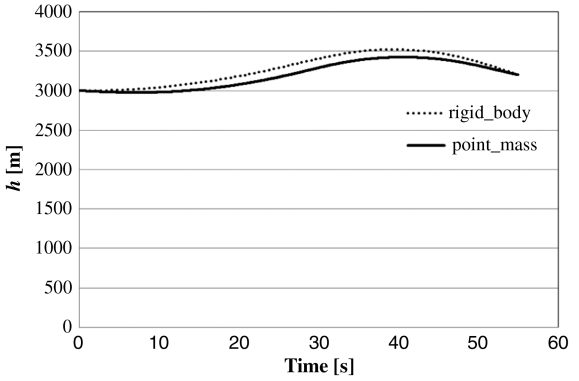

Fig. 18 Altitude histories (maneuver 2).

C. Maneuver 3

With the aircraft maintaining a velocity of 200 m/s and an altitude of 3000 m, the angle of the azimuth command ψ_c is given as follows:

$$\begin{aligned} \psi_c &= 0.0 \text{ deg} \quad && 0 \le t < 5.0 \text{ s} \\ \psi_c &= 30.0 \text{ deg} \quad && 5.0 \le t < 40.0 \text{ s} \\ \psi_c &= 0.0 \text{ deg} \quad && 40.0 \le t \le 65.0 \text{ s} \end{aligned} \tag{39}$$

In the previous two maneuvers there was no compensation term for the aircraft position; therefore, it is natural that deviations were caused between the trajectories obtained by the two models. In this case, the compensation term $(h_c - h)(k_4 s + 1)/(k_5 s + 1)$ is added to α_c in Fig. 3, and $k_{r3}(y_c - y)$ is added to β_c in Fig. 4, which reduce the deviations of the altitude and the lateral position between the two models, respectively. Figures 23 and 24 show the aircraft flight trajectories in the x-y plane and the altitude histories of the two models. In Fig. 23, the maximum difference between the two models

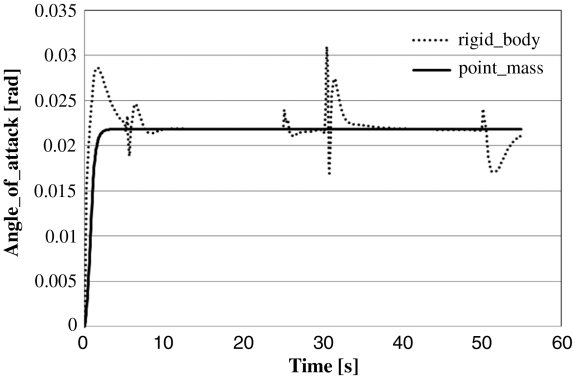

Fig. 19 Angle-of-attack histories (maneuver 2).

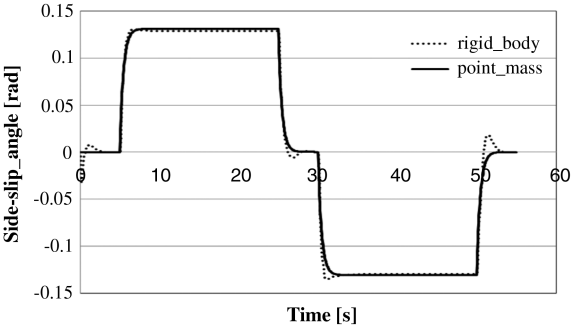

Fig. 20 Sideslip-angle histories (maneuver 2).

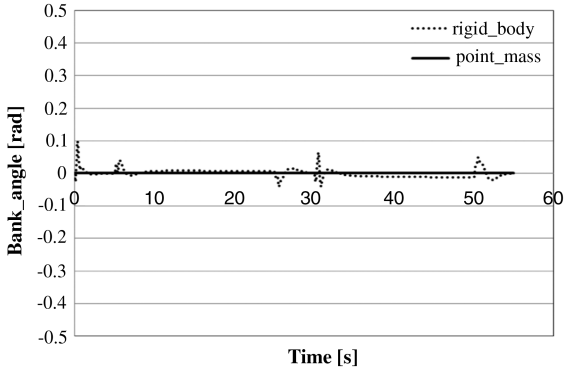

Fig. 21 Bank-angle histories (maneuver 2).

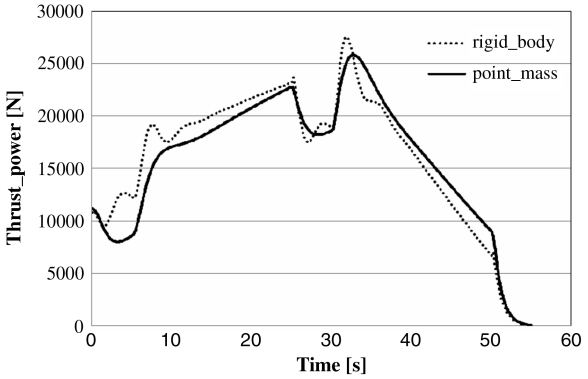

Fig. 22 Thrust histories (maneuver 2).

is about 30 m, which is far smaller than in the cases without the compensation term in β_c. In Fig. 24, the altitude histories of both models precisely follow the altitude command h_c (3000 m). The histories of the azimuth angle ψ by both models are almost the same in Fig. 25. In Fig. 26, the initial value of the α:α_0 in both models is 0, but in order to maintain the aircraft altitude at 3000 m, an α of 1.15 deg is required. The transient responses of the two models are a little different, but after 5 s, both histories are almost the same. The histories of β coincide with each other well in Fig. 27. In Fig. 28, small oscillations occurred in the rigid-body model by the change in the azimuth-angle command in Eq. (39). This is because in the rigid-body model, a roll-yaw coupling exists, while in the point-mass model, it does not exist. Both models employ the same engine model [15], and its thrust has a rather large time constant. The difference between the thrust histories in Fig. 29 is caused by this time constant; however, it is not large.

Calculating the optimal control of an aircraft by employing four control variables has now become possible. The original purpose of the study was to obtain optimal controls of an aircraft under windy

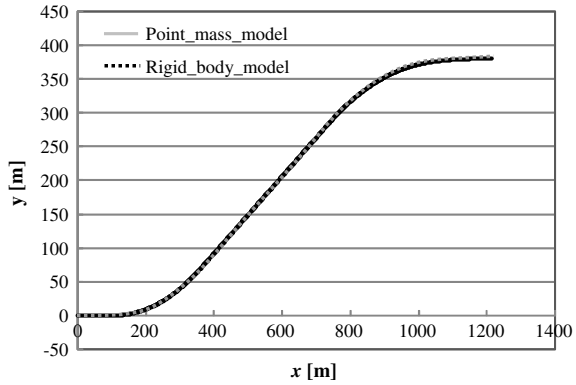

Fig. 23 Trajectories in the *x*-*y* plane (maneuver 3).

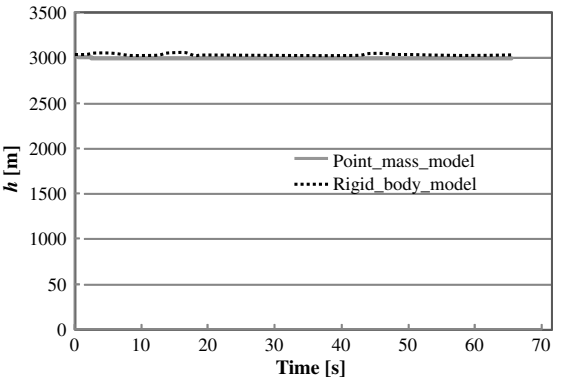

Fig. 24 Altitude histories (maneuver 3).

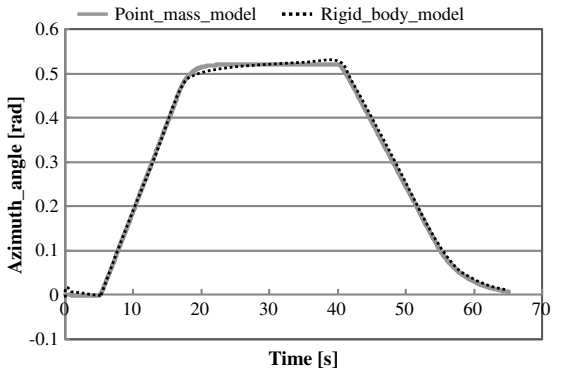

Fig. 25 Azimuth-angle histories (maneuver 3).

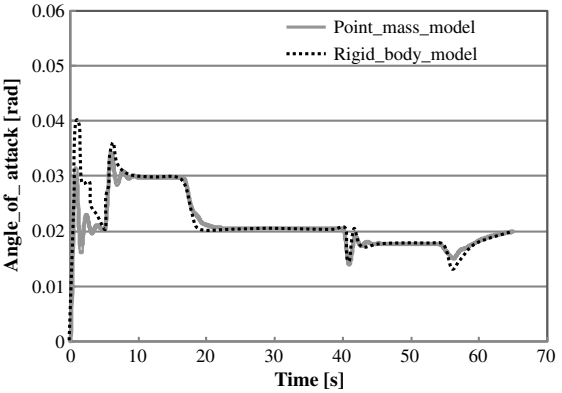

Fig. 26 Angle-of-attack histories (maneuver 3).

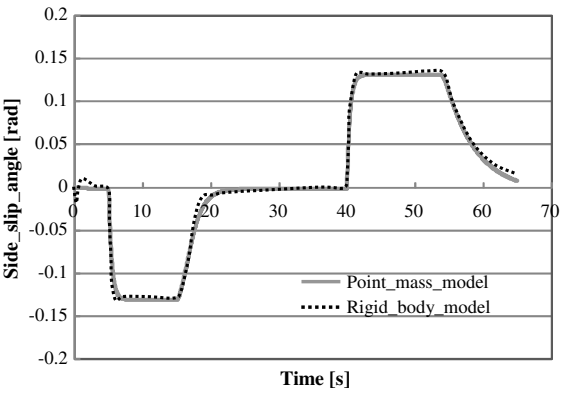

Fig. 27 Sideslip-angle histories (maneuver 3).

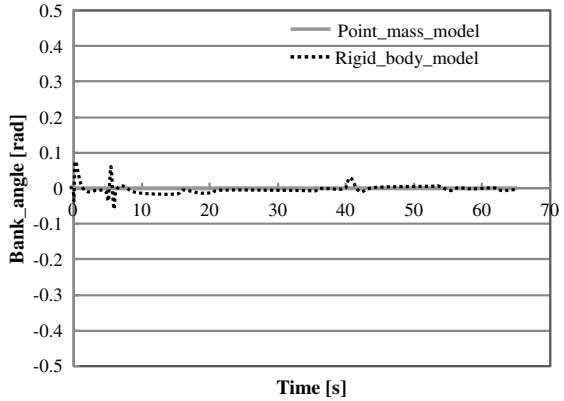

Fig. 28 Bank-angle histories (maneuver 3).

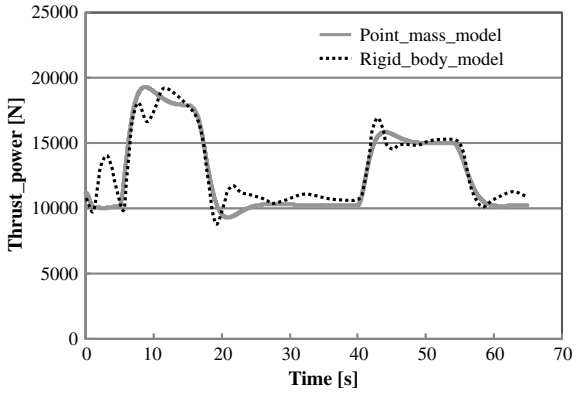

Fig. 29 Thrust histories (maneuver 3).

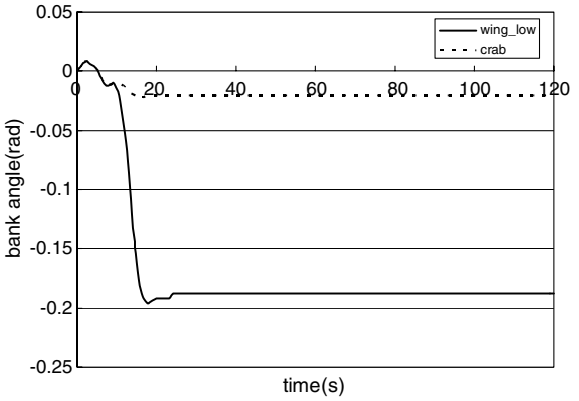

Fig. 32 Time histories of bank angles.

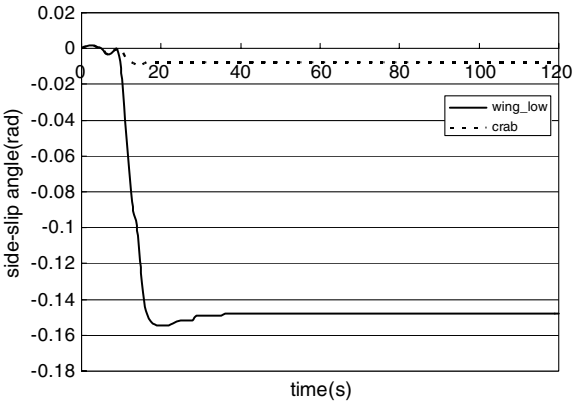

Fig. 33 Time histories of sideslip angles.

conditions; however, there are many studies left to be conducted. Here, only one example that shows the usefulness of the new point-mass model with four control variables is illustrated. Figures 30 and 31 are conceptual figures of aircraft landings with a crab flight and a wing-low flight. A crab flight is a flight to maintain the sideslip angle as zero, while a wing-low flight is a flight to maintain the aircraft attitude straight along the runway. When a cross wind exists, in a crab flight, the aircraft has to point its head in the direction of the relative wind, while in a wing-low flight, the aircraft can maintain its attitude and run a straight course by canceling the effect of the cross wind. Figures 32 and 33 show the bank-angle and the sideslip-angle histories in both landings. The sideslip angle is maintained to almost zero by the crab flight in Fig. 33, and the bank angle is small in Fig. 32. On the other hand, in the wing-low flight, these angles are actively controlled in order to progress along the runway without changing the aircraft heading. This wing-low flight simulation by a point-mass model only becomes possible by employing the new model developed in this study.

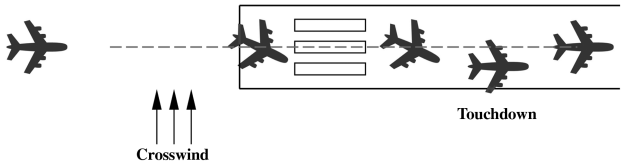

Fig. 30 Conceptual figure of landing by a crab flight.

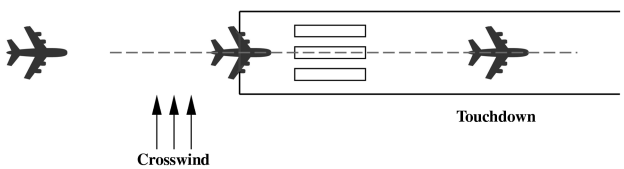

Fig. 31 Conceptual figure of landing by a wing-low flight.

V. Conclusions

A new aircraft point-mass model has been developed in the authors' laboratory. This model employs angle of attack, sideslip angle, bank angle, and thrust as four control variables and can introduce natural winds and active sideslip-angle control precisely. As the point-mass model is an approximation of a rigid-body model, the accuracy should be examined. For this purpose, some autopilot systems of the rigid-body aircraft had to be designed and incorporated into the rigid-body model so that it follows the command signal of the point-mass model. Next, the control-signal commands for step inputs and three typical aircraft maneuvers were applied to both the point-mass model and the rigid-body model, and the obtained aircraft motions were compared. The results show that the histories of control and state variables as well as the trajectories of both models coincided with each other well, and the applicability of this point-mass model was verified. Future research could include obtaining optimal aircraft maneuvers in dogfights or under windy conditions by employing the new point-mass model developed in this study.

References

[1] Hedric, J. K., and Bryson, A. E., Jr., "Minimum Time Turns for a Supersonic Airplane at Constant Altitude," *Journal of Aircraft*, Vol. 8, No. 3, March 1971, pp. 182–187. doi:10.2514/3.44251

[2] Uehara, S., Stewart, H. J., and Wood, L. J., "Minimum Time Loop Maneuvers of Jet Aircraft," *Journal of Guidance and Control*, Vol. 5, No. 5, Sept.–Oct. 1982, pp. 512–520. doi:10.2514/3.19783

[3] Lin, C. F., "Minimum Time Three-Dimensional Turn to a Point of Supersonic Aircraft," *Journal of Aircraft*, Vol. 8, No. 3, March 1971,

pp. 182–187.
doi:10.2514/3.44251

[4] Imado, F., and Miwa, S., "Fighter Evasive Maneuvers Against Proportional Navigation Missile," *Journal of Aircraft*, Vol. 23, No. 11, Nov. 1986, pp. 825–830.
doi:10.2514/3.45388

[5] Imado, F., and Miwa, S., "Fighter Evasive Boundaries Against a Missile," *Computers and Mathematics with Applications*, Vol. 18, Nos. 1–3, March 1989, pp. 1–14.
doi:10.1016/0898-1221(89)90120-X

[6] Imado, F., "Some Aspects of a Realistic Three-Dimensional Pursuit-Evasion Game," *Journal of Guidance, Control, and Dynamics*, Vol. 16, No. 2, March–April 1993, pp. 289–293.
doi:10.2514/3.21002

[7] Imado, F., and Ishihara, T., "Pursuit-Evasion Geometry Analysis Between Two Missiles and Aircraft," *Computers and Mathematics with Applications*, Vol. 26, No. 6, June 1993, pp. 125–139.
doi:10.1016/0898-1221(93)90122-C

[8] Imado, F., and Miwa, S., "Missile Guidance Algorithm Against High-*g* Barrel Roll Maneuvers," *Journal of Guidance, Control, and Dynamics*, Vol. 17, No. 1, Jan.–Feb. 1994, pp. 123–128.
doi:10.2514/3.21168

[9] Imado, F., and Uehara, S., "High-g Barrel Roll Maneuvers Against Proportional Navigation From Optimal Control Viewpoint," *Journal of Guidance, Control, and Dynamics*, Vol. 21, No. 6, Nov.–Dec. 1998, pp. 876–881.
doi:10.2514/2.4351

[10] Kinoshita, T., and Imado, F., "The Application of an UAV Flight Simulator—The Development of a New Point Mass Model for an Aircraft," *SICE-ICASE International Joint Conference 2006*, Paper FE-18-3, 2006.

[11] Lee, S., and Bang, H., "Three-Dimensional Ascent Trajectory Optimization for Stratospheric Airship Platforms in the Jet Stream," *Journal of Guidance, Control, and Dynamics*, Vol. 30, No. 5, Sept.–Oct. 2007, pp. 1341–1352.
doi:10.2514/1.27344

[12] Wickenheiser, A., and Garcia, E., "Optimization of Perching Maneuvers Through Vehicle Morphing," *Journal of Guidance, Control, and Dynamics*, Vol. 31, No. 4, July–Aug. 2008, pp. 815–823.
doi:10.2514/1.33819

[13] Dai, R., and Cochran, E. H., Jr., "Three-Dimensional Trajectory Optimization f in Constrained Airspace," *Journal of Aircraft*, Vol. 46, No. 2, March–April 2009, pp. 627–634.
doi:10.2514/1.39327

[14] Arrow, A., "An Analysis of Aerodynamic Requirements for Coordinated Bank-to-Turn Autopilots," NASA CR-3644, 1982.

[15] Gilbert, W. P., Nguyan, L. T., and Gunst, R. W., "Simulator Study of Effectiveness of an Automatic Control System Designed to Improve the High-Angle-of-Attack Characteristics of a Fighter Airplane," NASA TN-8176, May 1976.

[16] Ciuryla, M., Liu, Y., Farnworth, J., Kwan, C., and Amitay, M., "Flight Control Using Synthetic Jets on a Cessna 132 Model," *Journal of Aircraft*, Vol. 44, No. 2, March–April 2007, pp. 642–653.
doi:10.2514/1.24961

[17] Lampton, A., and Valasek, J., "Prediction of Icing Effects on the Curved Dynamic Response of Light Airplanes," *Journal of Guidance, Control, and Dynamics*, Vol. 31, No. 3, May–June 2008, pp. 656–673.
doi:10.2514/1.31165

[18] Shuette, A., Einarsson, G., Raichle, A., Schoening, B., and Moennich, W., "Numerical Simulation of Maneuvering Aircraft by Aerodynamic, Flight-Mechanics, and Structural Mechanics Coupling," *Journal of Aircraft*, Vol. 46, No. 1, Jan.–Feb. 2009, pp. 53–64.
doi:10.2514/1.31182

[19] Sonneveldt, L., Oort, E. R., Chu, Q. P., and Mulder, A., "Nonlinear Adaptive Trajectory Control Applied to an F-16 Model," *Journal of Guidance, Control, and Dynamics*, Vol. 32, No. 1, Jan.–Feb. 2009, pp. 25–39.
doi:10.2514/1.38785